DESIGN OF LONG IRIS-LOADED LINACS

R. B. Neal
Stanford Linear Accelerator Center

Before discussing recent work a short review* of the Stanford two-mile electron accelerator will be given. The present status is such that active construction has just begun since the contract with the AEC was completed in April, 1962. It is interesting to note that this is about 5 years from the date when the first proposal was submitted. Present schedules call for completion of the accelerator and start of the experimental program in July, 1966.

The main parameters for this machine are given in Table 1. Authorization has been obtained to build Stage I, as indicated, of the accelerator. Depending on subsequent authorization, the next step would be Stage II, which would require additional power with the same length of the machine. The accelerator will be built in 30 sections of 333-1/3 feet each, located underground. Above the accelerator housing is a klystron gallery which will contain all the equipment requiring periodic maintenance. In this fashion it is hoped to attain ultimately a 24-hour per day operating schedule. A more detailed cost breakdown of the accelerator proper follows:

---

* A useful list of references has been given in "Linear Accelerator Conference Report", BNL, IA AvS-1, April 1961

TABLE 1

THE STANFORD TWO-MILE LINEAR ELECTRON ACCELERATOR

Site	480	acres
Conventional Building Space	251,000	square feet
Accelerator Length	10,000	feet
Beam Energy		
Stage I	10 - 20	Bev
Stage II	20 - 40	Bev
Project Power Demand	50	megawatts
Total Staff	730	
Construction		
Beginning	June, 1962	
Completion	July, 1966	
Pre-Construction Research and Development Costs	$ 18	million
Construction Costs (including engineering, design, inspection, and management fees)-5/62 estimate		
Site, Buildings, and Utilities	37.8	million
Accelerator and Associated Equipment	45.0	million
Beam Switchyard and Research Equipment	8.3	million
Escallation and Contingency	22.9	million
TOTAL CONSTRUCTION COST	$114.0	million
Annual Operating Cost	$ 20.0	million/year
Operating Schedule	24	hour/day
Sponsor	U. S. Atomic Energy Commission	

Proceedings of the 1962 Conference on Linear Accelerators for High Energies, Upton, New York, USA

End station shielding	$ 1.0	10^6
240 klystrons	2.2	10^6
240 modulators	6.2	10^6
Dc supplies	1.7	10^6
Accelerator structure	3.2	10^6
Waveguides ($20/foot for copper waveguide)	4.5	10^6
Rf system	2.4	10^6
Vacuum	3.4	10^6
Etc., etc.	7.4	10^6
Total	$32.0	10^6

The accelerator Stage I and Stage II specifications are listed in Table 2. It is contemplated that the machine should be able to handle as many as six simultaneous beams emerging at different energies. Initially it is proposed to have only two such beams at different energies.

Experience shows that every machine that has been built eventually has become very crowded in the target area, therefore, 150 acres have been reserved for this purpose. Initially one target building for scattering experiments and another for production of secondary particles is contemplated.

The basic concept of dividing the output power from a klystron to feed an accelerator section for Stage I is shown in Fig. 1. All the necessary waveguides are installed such that eventually only additional klystrons have to be connected to complete Stage II. The Project M klystron will be improved as compared with those used on the Mark III accelerator. The number of cavities will be increased from 3 to 5; thus it is possible to increase the gain from 35 to 50 db and hopefully the efficiency from 30 to 38%. The peak power will be increased from 17 Mw to 24 Mw. Also,

TABLE 2

GENERAL ACCELERATOR SPECIFICATIONS

	Stage I	Stage II	Notes
Accelerator Length	10,000 feet	10,000 feet	
Length Between Feeds	10 feet	10 feet	
Number of Accelerator Sections	960	960	
Number of Klystrons	240	960	
Peak Power per Klystron	6-24 Mw	6-24 Mw	
Pulse Repetition Rate	1-360 pps	1-360 pps	1
R F Pulse Length	2.5 μsec	2.5 μsec	2
Electron Energy, Unloaded	11.1-22.2 Bev	22.2-44.4 Bev	3
Electron Energy, Loaded	10-20 Bev	20-40 Bev	3
Peak Beam Current	25-50 ma	50-100 ma	4
Average Beam Current	15-30 μa	30-60 μa	4
Average Beam Power	0.15-0.6 Mw	0.6-2.4 Mw	4
Filling Time	0.83 μsec	0.83 μsec	
Electron Beam Pulse Length	0.01-2.1 μsec	0.01-2.1 μsec	5
Electron Beam Energy Spread (max)	± 0.5%	± 0.5%	6
No. of Electron Energy Levels (max)	6	6	
Accelerator Vacuum	$< 10^{-5}$ mm of Hg	$< 10^{-5}$ mm of Hg	
Operating Frequency	2856 Mc/sec	2856 Mc/sec	7
Operating Schedule	24 hrs/day	24 hrs/day	8

Neal
July 1960

pulse length will be increased from 2.0 to 2.5 microseconds. The klystron average power output will be raised as a result of the longer pulse length and the increase of repetition rate from 60 to 360 pulses per second. These klystrons will have fixed tuning and probably permanent magnets for beam focusing in contrast to the adjustable tuning and electromagnetic focusing which characterizes the Mark III klystrons.

The number of modulators will be quadrupled as Stage II comes into operation. In order to obtain 24 Mw output from each klystron, each of the modulators must put out 64 Mw peak power, based on the planned conversion efficiency of 38% of each klystron.

Close operating tolerances are necessary on the modulator; the pulse height may not deviate from flatness by more than 0.5%, and the pulse to pulse variation may not deviate by more than 0.25%. In order to meet these requirements, some changes have been made in modulator circuitry. One of these is the "de-Q-ing circuit", which will clamp the modulator output voltage by comparing it to an adjustable reference voltage. Such a circuit wastes power, so a "scavenging circuit" has been added, which in effect returns the unused power to the dc line. The operation of the "de-Q-ing" and "scavenging" circuits is as follows: the dc line is filtered and charges up the pulse forming network through a type of transformer, called a "transactor" (in place of the usual choke) and a diode. As the line is charged, a portion of the charging voltage is taken off and compared to a reference voltage. When the reference voltage is reached, a thyratron switch is triggered, dumping the energy stored in the "transactor" over into the filter on the primary side. The reference voltage of the modulator can be adjusted at the console. It is contemplated to use the reference voltage to at least one of the sectors to "servo" the beam energy and thus to achieve precise energy control.

Several types of drive lines are possible. One idea under consideration is to operate the drive line in a cw fashion, because of the requirement that the phase shift between the wave on the drive line and the electron beam should not exceed 18° along the two miles, and this is most readily accomplished by a cw drive. However, using 2856 Mc/s, either the line has to be very large to reduce losses or boosters have to be used. Pulsed boosters are more likely to shift phase than are cw boosters. However, it is believed that a pulsed drive line could be maintained within the tolerances, because of the relatively low power level, i.e., 50 kw. The possibility of operating the drive line on the 24th subharmonic of 2856 Mc/s, i.e., 119 Mc/s, and putting in frequency multipliers at each of the 30 sectors is being examined. This system requires no in-line boosters. A small sub-booster (klystron) is used to amplify the reconstituted frequency and provide drive power for all the klystrons in each sector in either Stage I or Stage II.

The conventional technique of phasing this machine consists of adjusting the input rf phase at each klystron while observing and maximizing the output energy. On the Mark III each of 30 such sources add, so one has about a 3% effect from each source. But on the two-mile accelerator, each klystron contributes something like one part in a thousand of the total beam energy, or one part in 240 in our Stage I machine. Therefore, alternate techniques that have good sensitivity but which do not depend upon the number of sources have been examined. A method that depends upon a local effect is desired and therefore several varieties of beam interacting techniques have been studied. One method consists of momentarily turning off the rf power to the particular section being phased and allowing the power from the beam-induced wave only to pass through, using this to establish a phase

reference; then the rf power is turned on and the externally impressed rf wave is set 180° away from the induced wave. This is a very sensitive technique since the induced wave in the accelerator section is an exponentially growing wave. In fact, there is much greater sensitivity than could be achieved using a single cavity. Furthermore, all of the devices needed are already built in, since the induced wave is set up in the accelerator section itself.

An alternate phasing technique that is somewhat less cumbersome but also somewhat less accurate is shown in Fig. 2. In this case one compares the output phases of succeeding accelerator sections in a phase detector, each line being separated by isolators. One periodically turns off the rf and, making use of the waves induced by the beam, establishes a null which in effect makes the line lengths through each accelerator section to the detector electrically equal. This provides a means of obtaining a quick check of the phase information and also provides a way of adjusting the phase quickly when a new klystron is installed.

Compensating for what has been called transient beam loading has been studied and a corrective technique is as follows. When the first particles go through the accelerator they see an unloaded condition; the entire stored energy in the accelerator is still present and therefore the beam comes through with maximum energy. As the particles subtract stored energy from the structure, the beam energy drops off until it finally reaches the steady state case after one filling time. A corrective technique involves "turning on" the rf power to accelerator sections down the line in a stepwise manner. In a particular example, the entire number of sectors were divided into three parts and they were turned on at slightly different times. In this manner energy compensation can be obtained and can greatly reduce

the energy spread of the beam. Division into more parts than three can be done, of course, with consequent smaller energy spread.

The foregoing has been primarily a review. In the following, some recently measured characteristics of accelerator structures will be presented. A typical waveguide structure is shown in Fig. 3. Two particular cases shown have been investigated. One type cavity has a conical disk, the narrow part being on the inside; another type has been referred to as "anti-conical" in which the thick part of the disk is on the inside. Shunt impedance measurements have been made for both of these types as well as for the type with the flat disk. It was found that the conical design (for a given aperture) is actually lower in shunt impedance by roughly 5%, compared to the case where the disk is flat. The anti-conical type results in an increase by roughly 5%. However, this latter case is no better than that of the flat disk where the thickness is equal to the narrow part of the anti-conical iris. It can be stated that the advantage that one would get from the anti-conical construction would not be worth the increased cost of machining the disk in such a fashion.

The coupling aperture into the side of a 10-foot accelerator section is shown in Fig. 4. The plotted curve, as shown, represents the E_z field across the aperture. Without the iris the field would be approximately flat. With the iris the H-field in effect bows out. It results in an asymmetrical characteristic E_z across the aperture in the fashion shown. The difficulty with the non-uniform E_z is that as the beam passes through with a slight phase spread there is a coupling between the phase spread and the transverse momentum given to the particle as it passes through. Therefore, on the long accelerator some concern existed about this, because if all of these effects were additive, the beam would come out of this machine with a large increase

in the angular spread. Ways have been found to flatten the E_z. One very simple way consists of offsetting the coupler cavity in the manner shown in Fig. 4. This corresponds to roughly 0.050 inch offset of the coupler cavity axis, while keeping the aperture in line with all the other apertures. Almost perfect compensation has been obtained. To obtain a second order correction, all of the input power to the sections are brought in on one side, taking all the output power off the other side.

Theoretical and experimental curves of shunt impedance versus the number of disks per wavelength for various disk thicknesses are shown in Fig. 5. The full lines represent the calculated curves, and the dotted lines represent the experimental curve. For zero disk thickness the optimum occurs at approximately 3-1/2 disks per wavelength. As the disk thickness increases the optimum number of disks per wavelength shifts to the left, and becomes equal to 3 for a disk thickness of 0.120 inches and equal to about 2.7 for a disk thickness of 0.230 inches. The disk thickness adopted for the two-mile accelerator is 0.230 inches. The theoretical results indicate thinner disks but cavity experiments with these have shown difficulty due to internal arcing. Also, 3 disks per wavelength have been adopted in contrast to n = 4, the number of disks per wavelength used in earlier Stanford accelerators. This increases the shunt impedance by about 10%. The experimental shunt impedance value shown here is around 60 as compared to the theoretical value of about 90. This is because the theoretical curves do not properly take into account the aperture in the disk and the theoretical values of conductance for copper were used.

Investigations of shunt impedance variations as a function of group velocity in the structure yielded results as shown in Fig. 6. The group velocity varies roughly as the fourth power of the disk aperture. The next

step is to carry out the harmonic analysis for each case. The resultant curves for $a_o^2/\Sigma a_n^2$ are also shown in Fig. 6. The a_o is a coefficient corresponding to the fundamental wave, a_n to the nth spatial harmonic. The curve for the ratio indicated above shows how the fraction of the power carried in the fundamental space harmonic drops off as one goes to lower group velocities. Combining the curves shown results in values for r_o/Q, corresponding to the fundamental space harmonic, as a function of group velocity. This is also indicated in Fig. 6. For example, for a group velocity of 0.01, the value for r_o/Q is approximately 40 meg/meter. Multiplying this by the Q value, obtained from another measurement, yields the fundamental spatial harmonic shunt impedance, r_o.

It was decided to use a constant gradient accelerator structure in contrast to the constant attenuation (or constant impedance) structure. The constant impedance accelerator structure is obtained when all the cavity dimensions are uniform along the entire section. In this case, one obtains an exponential decrease in the power flowing through the structure and in the electric field along the length as shown in Fig. 7. One of the bad features of this design is that the highest field occurs at the input end and therefore when one has a limitation due to breakdown it occurs at $z = 0$. On the other hand, the peak field is always well above average field. This would limit the achievable output energy. The constant gradient case is obtained by varying the structure dimensions along the length. In the particular method used, the group velocity of the structure is varied in a linear manner from the input end to the output end. In this manner uniform axial electric field strength along the accelerator is obtained, which is an advantage over the constant impedance case if higher energy levels are desired. In terms of shunt impedance the constant gradient structure also

has a 2 or 3% higher effective shunt impedance. A detailed price estimate shows that a 10-foot constant gradient section costs only 10% more than an equivalent constant attenuation section. In the light of the cost of the accelerator proper as compared to the cost of the entire machine, this reflects only a rather small increase of the total cost.

A comparison of the constant gradient structure and the constant attenuation structure on the basis of various characteristic parameters is given in Table 3. For the particular design under consideration, the variation of cavity and disk aperture dimensions, group velocity and corrected shunt impedance as a function of distance along a 10-foot constant gradient section is shown in Fig. 8. Q value measurements, evaluated as indicated before, have been done for this case and the trend is shown in Fig. 9, varying from about 14,000 to approximately 13,000 over the 10-foot section.

One of the advantages of the constant gradient structure over the constant attenuation structure is that there is less tendency to build up and propagate some of the higher order modes. As is well known, the electron accelerator has been plagued with the phenomenon that has been called variously "beam breakup" and "pulse shortening". This is now thought to be due to a buildup of power, in a higher order passband of the TM_{11} mode. This results in a backward wave mode with pronounced transverse electric field. The magnitude of this field increases with increasing beam current. So a threshold is reached if the beam current is such that the transverse field is sufficient to sweep the beam out. Increasing the beam current will therefore result in a corresponding shortening of the pulse. Experimental observation shows that the total charge in the beam pulse (as limited by pulse shortening) remains about constant.

TABLE 3

Comparison of constant gradient (c.g.) and constant attenuation (c.a.) accelerator structures at $\alpha\ell = 0.6$

Characteristic	Constant Gradient	Constant Attenuation	Ratio c.g./c.a.
Ratio of peak to average electric field	1.0000	1.3298	0.752
Ratio of rf power loss at input to rf power loss at output of section	1.0000	3.3201	0.301
No-load (zero-current) energy	11.772 Bev	11.600 Bev	1.015
Energy decrease at 50 ma peak current	1.662 Bev	1.708 Bev	0.973
Energy at peak current of 50 ma	10.110 Bev	9.892 Bev	1.022
Maximum beam conversion efficiency	0.724	0.684	1.058
Current at max. efficiency	177.1 ma	169.8 ma	1.043
Normalized group velocity	.0201 → .0061	0.0117	1.718 → 0.521
Filling time	0.872 μsec	0.872 μsec	1.000
Stored energy	731.2 joules	731.2 joules	1.000
Phase shift at 10 ft for frequency change of 0.1 Mc/sec	0.546 rad	0.546 rad	1.000
Relative energy loss for frequency change of 0.1 Mc/sec	0.0357	0.0424	0.842

Assumed parameters

Attenuation per section: 0.6

Total input power: 1440 Mw

Total length: 9600 ft (293,000 cm)

No. of sections: 960

Length per section: 10 ft (305 cm)

Angular frequency: 1.79×10^{10} rad/sec

Shunt impedance: 0.47×10^{6} ohms/cm

$Q_0 = 13{,}000$

Experience with two accelerators, using a constant gradient structure, has indicated that there is not the strong buildup of the TM_{11} mode as with the uniform structure. The reason is that the passband for the high order mode varies along the length of the structure. This has been indicated in Fig. 10. At the input end the passband lies between 4124 and about 4320 Mc/s. Halfway down the section, the passband lies between 4246 and about 4390 Mc/s, while at the output end the passband is still narrower, i.e., 4335 to 4420 Mc/s, and higher than at the other points along the section. The $v_p = C$ line shown corresponds to a different frequency in each of these regions, and thus the strong coupling and strong buildup of the TM_{11} mode is avoided, because of the different frequency intersection at each point. This is thought to be the explanation why the constant gradient structure is not subject to pulse shortening. It is probably not of importance for the two-mile accelerator, although it could become so at very high beam currents.

Some study has been devoted to another type of transient effect. New observations have been made related to the transient behavior of the rf pulses in the constant gradient structure and in the constant attenuation structure. Recently, experiments done with the NBS machine have shown that ripples are generated on the leading edge of the rf pulse as it passes through an accelerator section. Some calculations were done on this phenomenon by J. Leiss and an explanation based on filter circuit theory was obtained that corresponds very well with the observed behavior. In effect, since the accelerator structure is a passband filter, the imposition of an rf pulse of finite rise time will result in many components of frequency propagating in the structure, in addition to the fundamental frequency. These various frequencies have different phase velocities, those with frequencies higher than the fundamental frequencies are propagated with phase velocities less than the velocity of light, and vice versa. These waves mix inside the structure and the output

pulse exhibits the ripples mentioned above. In addition, it was shown by J. Leiss that in the $\pi/2$ case, in the middle of the passband, only amplitude distortion of the output wave is obtained. On the other hand in a region away from the center, for example, in the $2\pi/3$ case, not only an amplitude distortion but also a phase distortion is obtained in the output wave. Measurements at Stanford have shown that in the $2\pi/3$ case there is somewhat less distortion in the wave form for the constant gradient case than for the constant impedance case. In the present experiments, the distortions shown in Fig. 11 were exaggerated because the power source produced a variable frequency and a variable phase during the rise time. Other data show a much less pronounced effect if one uses, for instance, an rf switch controlling a cw amplifier to supply pulses of rf power.

This effect is not too troublesome, but it does cause an energy variation of the order of 2 to 3% of the particles passing through the machine when the transient waves are still present. The distortions in the $2\pi/3$ case, according to the calculations of J. Leiss, do not lead to any greater energy spread; in both the $\pi/2$ case and $2\pi/3$ case, it is about the same, of the order of 1 to 3%. Calculations are now being done on the constant gradient case.

Building almost 1000 accelerator sections in a period of a year and a half to two years, makes it necessary to think very seriously about the fabrication techniques to use, the cost of these techniques, the methods of quality control, etc. Two techniques have been investigated for fabrication of the accelerator sections. These are the electroforming technique and the brazing technique. In the electroforming method the entire stack of parts comprising a 10-foot section are stacked on a mandrel. This array consists of copper disks separated by aluminum spacers; the spacers being of just the correct

size to separate the disks by the right amount. This entire array of disks and spacers is then set horizontally into a copper sulfate electroforming solution, in such a way that half of the metal surface is exposed and half is underneath the surface of the bath. The assembly is caused to rotate at a speed of around 30 rpm. While it is rotating, agate burnishing tools move slowly back and forth along the surface in the axial direction. The purpose of the burnishing tools in the electroforming process is removal of the tiny spikes that tend to build up and thus to prevent the growth of what are called "trees". This technique has permitted speeding up the electroforming process to such an extent that it is now possible to electroform a 3/8 inch wall on a copper tube of this size in 9 days time, in contrast to 6 weeks time required when this development was first started. When electroforming is completed the external surface has a very fine, satiny finish. After removal of the section from the electroforming solution, the aluminum spacers are etched out in a sodium hydroxide solution and an all-copper structure remains in which the crystal structure is continuous across the boundary between the disks and the wall, and the disks are thus strongly bonded to the wall.

The brazing technique is accomplished in a furnace, as shown in Fig. 12, that has been developed for this purpose exclusively.

A ring burner with a hydrogen-oxygen flame is used. During the brazing operation a reducing atmosphere is supplied on both inside and outside of the accelerator section to prevent corrosion. The entire brazing procedure takes less than 3 hours. On the basis of this, it has been decided tentatively to use the brazing technique for manufacturing the accelerator sections for the two-mile machine.

The electroforming technique is basically the more accurate of the two methods. However, in either case, it is necessary to tune the sections after

fabrication because of the close tolerances required. A split ring is placed around a section and a dimpling tool squeezes against the outer wall as the operator observes the phase shift pattern. In this manner one can, using a shorting plunger, tune each cavity independently along the length of a section. Each cavity can be tuned to better than 1^{o} in phase, so that a tolerance of 5^{o} phase excursion over a whole 10-foot section can be obtained. The dimples are visible externally because the copper is very soft. However, looking at the inside it is impossible to see the dimple because a deformation is made of this wall of the order of one ten-thousandth of an inch.

Some recent results obtained by D. Chang, A. Kirschbaum, G.A. Loew and R.B. Neal, which are pertinent to the design of a proton accelerator, are given in Table 4. This tabulates the results of measurements of shunt impedance versus normalized phase velocity for a disk-loaded waveguide, with the phase velocity varying from 0.5 to 1.0. The experimental conditions were: mode $2\pi/3$; frequency 2856 Mc/s; constant disk aperture $2a = 0.890$ inches; disk thickness $t = 0.230$ inches; rounded edges on the inner part of the apertures. One sees in the table that the disk spacing varies along the length in a linear way: 0.689 inch spacing at $\beta = 0.5$ up to 1.378 inch at $\beta = 1.0$. The 2b diameter varies by a small amount, from 3.339 up to 3.245 inches. Interestingly, the group velocity varies only slightly, from $v_g/c = .0097$ at the low β to .0116 at β equal to unity. This is significant for proton accelerators in that there can be a large number of sections with the same aperture throughout and they all have essentially the same filling time per unit length. If this were not true, one might find it necessary to vary the disk apertures in the different sections. The tabulated results are graphically illustrated in Fig. 13, showing that the useful shunt impedance varies from about 10 meg/meter to 54 meg/meter.

TABLE 4

$\beta = v_p/c$	0.5	0.6	0.7	0.8	0.9	1.0
Disk spacing d (in)	0.689	0.827	0.965	1.102	1.240	1.378
Diameter 2b (in)	3.339	3.307	3.287	3.270	3.254	3.245
v_g/c	0.0097	0.0110	0.0116	0.0116	0.0120	0.0116
$(r/Q)_{total}$	17.3	25.8	31.8	39.3	45.1	49.8
$a_o^2/\Sigma a_n^2$	0.89		0.834		0.860	0.850
$(r/Q)_o$ *	14.35	21.41	26.4	32.65	37.5	41.4
$Q_{theoretical}$ **	6950	8480	9770	10980	12030	13000
Q exp. on 3 cavities	2195	2380	3395	3415	4590	4335
$r_o = (\frac{r}{Q})_o Q_{th} (\frac{M\Omega}{m})$	9.98	18.19	25.80	35.80	45.2	53.8

* Based on an average value of $\frac{a_o^2}{\Sigma a_n^2} = 0.83$

** Based on $\frac{Q\,\delta}{\lambda_o} = \frac{\beta\,(1-\eta)}{n + 2.61\beta\,(1-\eta)}$ where $\eta = t/d$ and $n = 3$

Proceedings of the 1962 Conference on Linear Accelerators for High Energies, Upton, New York, USA

Discussion

L. Smith (LRL): Would you eventually have to move or modify the target buildings when Stage II is completed?

R.B. Neal (Stanford): Those immediately planned are for 20 Bev beams. Later additional buildings and target sites will be added and will be located in a "Christmas tree" fashion.

L. Smith (LRL): Can Stage II be completed in steps?

R.B. Neal (Stanford): Yes. Power sources can be added in an incremental fashion.

J.P. Blewett (BNL): Do you have figures for power losses in the coupling waveguides for the accelerator?

R.B. Neal (Stanford): Losses are roughly 5%; this amounts to approximately 0.006 db/ft.

J.P. Blewett (BNL): What are the phase shift stability specifications for the modulators?

R.B. Neal (Stanford): This is of the order of 1^{o} to 2^{o}.

H.B. Knowles (Yale): Does the "de-Q-ing" and "scavenging" circuit represent the only servo on the machine?

R.B. Neal (Stanford): It will be possible to adjust the energy reference voltage, but the feedback will be sent to just one sector. We will use the reference voltage as a general energy control. This has a control range of only 10%, so beyond this we must change the level of dc voltage.

J.P. Blewett (BNL): With what precision can you control phase?

R.B. Neal (Stanford): We think we can basically control phase within a degree or so. The complicating feature of this is that phasing is done with pulse power so one must have pulse-type phase detectors. Also present are the natural phase shifts coming from the klystrons due to beam voltage variations. Pulse type phase detectors have actually been used at low level power where one has very carefully controlled conditions; in this case it is possible to obtain accuracies of a tenth of a degree. We hope to be able to control phase within a few degrees, and have in fact established a tolerance of 5 degrees total.

K. Batchelor (Rutherford): Suppose you have beam loading and also want to operate at a phase angle of 30^{o} or so; how would one utilize the pulsed rf phase detector?

R.B. Neal (Stanford): You would probably find it better in that case to phase on the peak and then subsequently introduce your 30^{o} phase shift - this would be my offhand guess.

H.B. Knowles (Yale): Why do you use an iris in the coupler structure to the accelerator (ref. Fig. 6)?

R.B. Neal (Stanford): We use the iris in preference to other types of coupling because first of all, it is very simple to build, and secondly, useful acceleration is obtained in the coupling cavity which would not be obtained in the coaxial type couplers. When it is realized how precious length is to a machine of this type and that a coupling cavity of another sort might subtract 5 to 10% of this length then one sees the importance of using an iris feed.

L. Smith (LRL): With reference to Fig. 8, is the significance of r_o/r_T about that of the transit time factor?

R.B. Neal (Stanford): Yes. This is equivalent to putting in a transit time factor in the standing wave case.

R.L. Gluckstern (Yale): Do some of the values shown in Fig. 8 refer to the conical disk?

R.B. Neal (Stanford): We have some miscellaneous points plotted for the conical disk, but they were not used in any of the curves shown. Some of these points have bevelled edges on the aperture, some do not. The ones that were kept perfectly square are shown by the little squares. We find that the use of a bevelled edge results in about a 5% to 10% reduction in shunt impedance for a given aperture. However, if we normalize to a fixed group velocity we find there is essentially no change in the shunt impedance.

R.L. Gluckstern (Yale): Is the constant gradient structure designed for the case of absence of current?

R.B. Neal (Stanford): We will design to have a slightly increasing gradient in the absence of current (the unloaded case) such that it will become essentially uniform with design current loading.

R.L. Gluckstern (Yale): Is the iris spacing constant and is only the aperture changed for the adopted accelerator structure?

R.B. Neal (Stanford): The aperture spacing remains uniform in the case we have chosen.

R.L. Gluckstern (Yale): Is there a significant factor in the cost of doing it this way?

R.B. Neal (Stanford): It helps. Our studies have shown that it is cheaper to vary the aperture dimension than to vary the spacing.

K. Batchelor (Rutherford): Is there any special advantage to doing it this way?

R.B. Neal (Stanford): I think you are actually worse off if you vary the spacing because if you try to keep the aperture constant and vary the spacing I think that some fairly narrow aperture dimensions would be required and the Q would fall off badly.

K. Batchelor (Rutherford): Is it comparable to vary the spacing?

R.B. Neal (Stanford): The difficulty is that it is not possible to vary the disk spacing alone because in order to achieve the prescribed group velocity and the prescribed phase velocity it would be necessary to vary at least one other dimension.

L. Smith (LRL): What are the Q values for the cavities made by the electro-forming process?

R.B. Neal (Stanford): We get about 90% of the theoretical Q value.

J.P. Blewett (BNL): What is the tolerance on the cooling water temperature for the accelerator sections?

R.B. Neal (Stanford): We have to keep the water temperature to within $1/2^{o}C$ to maintain correct phase relations.

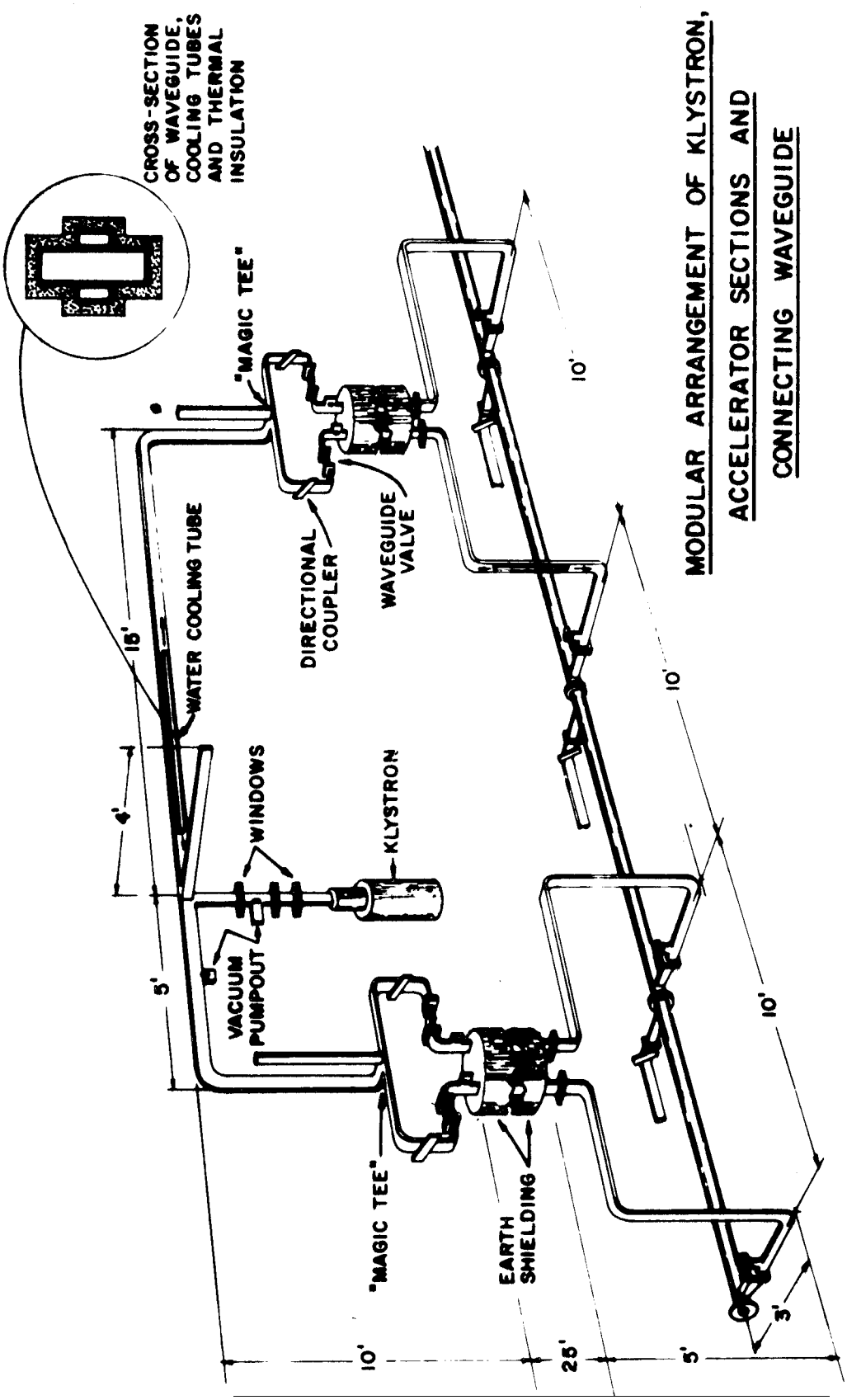
MODULAR ARRANGEMENT OF KLYSTRON, ACCELERATOR SECTIONS AND CONNECTING WAVEGUIDE
CROSS-SECTION OF WAVEGUIDE, COOLING TUBES AND THERMAL INSULATION
"MAGIC TEE"
WATER COOLING TUBE
DIRECTIONAL COUPLER
WAVEGUIDE VALVE
WINDOWS
KLYSTRON
VACUUM PUMPOUT
"MAGIC TEE"
EARTH SHIELDING
10'
10'
10'
10'
25'
5'
3'
15'
4'
5'

Fig. 1

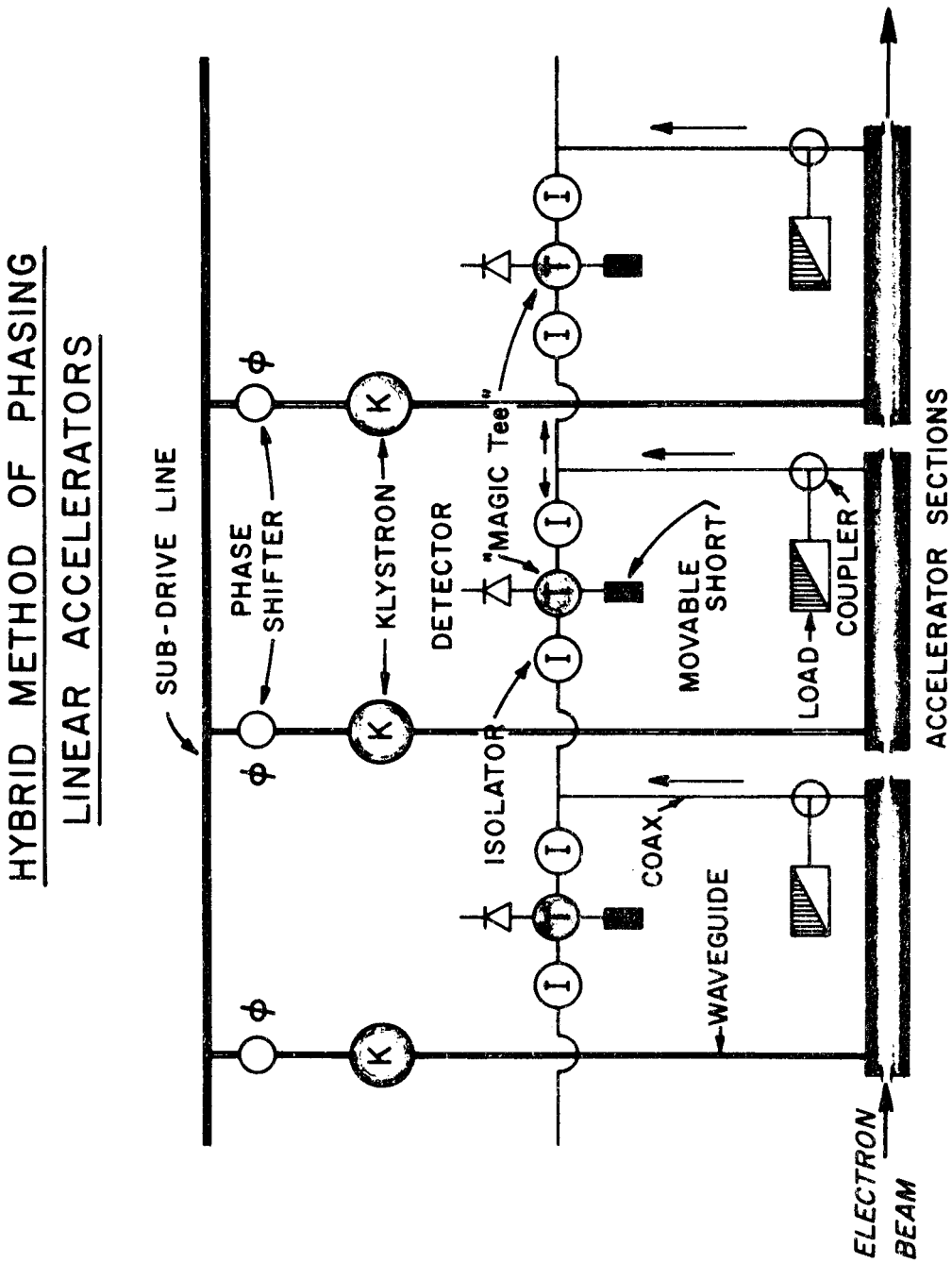
HYBRID METHOD OF PHASING
LINEAR ACCELERATORS
SUB-DRIVE LINE
PHASE SHIFTER
KLYSTRON
DETECTOR
"MAGIC Tee"
ISOLATOR
COAX
WAVEGUIDE
MOVABLE SHORT
LOAD
COUPLER
ACCELERATOR SECTIONS
ELECTRON BEAM

Fig. 2

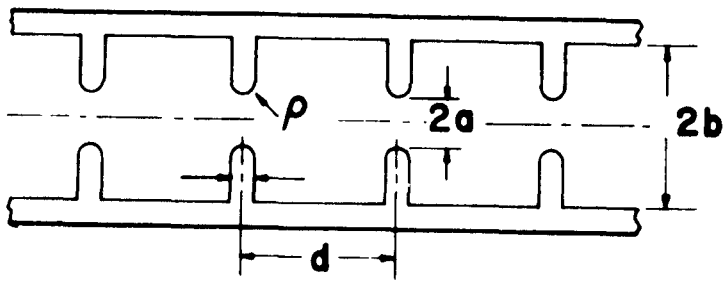

a) TWO UNIT CELLS

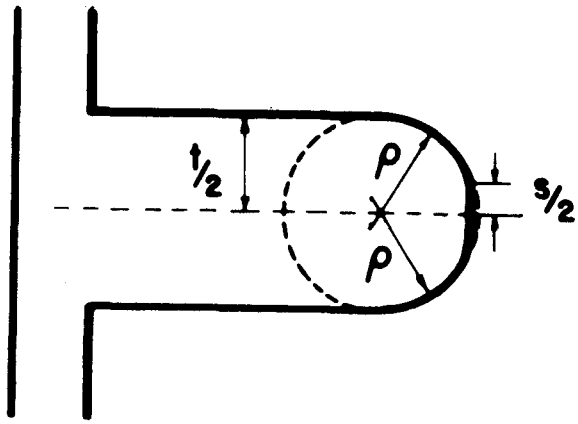

b) ILLUSTRATION OF DISK

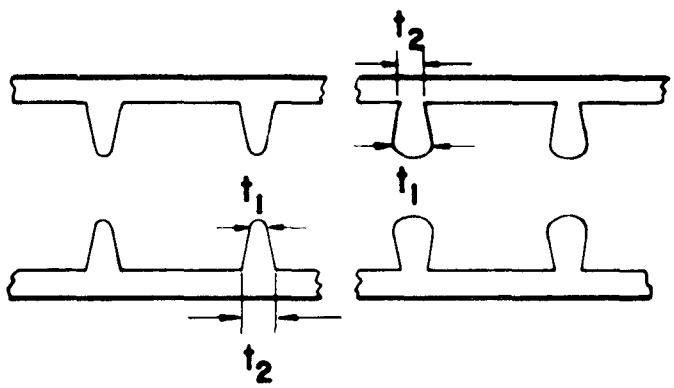

c) "CONICAL" AND "ANTICONICAL" DISKS

Fig. 3 - SCHEMATIC DRAWING OF DISK-LOADED WAVEGUIDE.

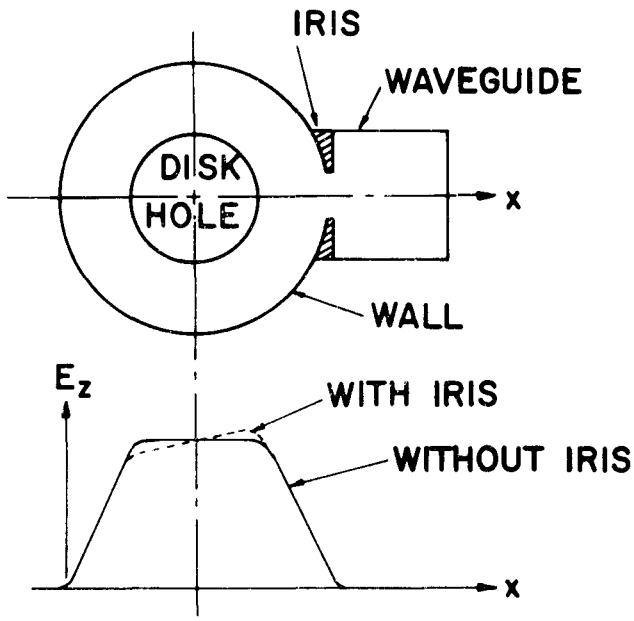

a) COUPLER CROSS-SECTION AND CORRESPONDING LONGITUDINAL ELECTRIC FIELD INTENSITY.

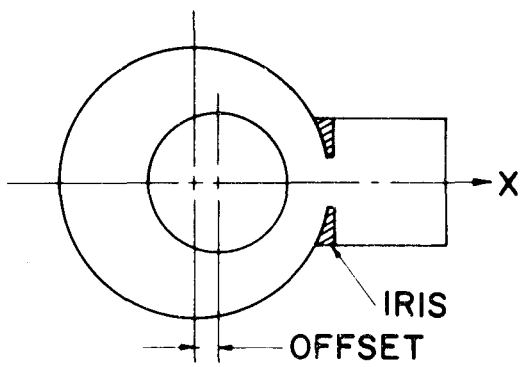

b) COUPLER SHOWING OFFSET TO CORRECT FIELD ASYMMETRY.

Fig. 4 - COUPLER ASYMMETRY STUDIES

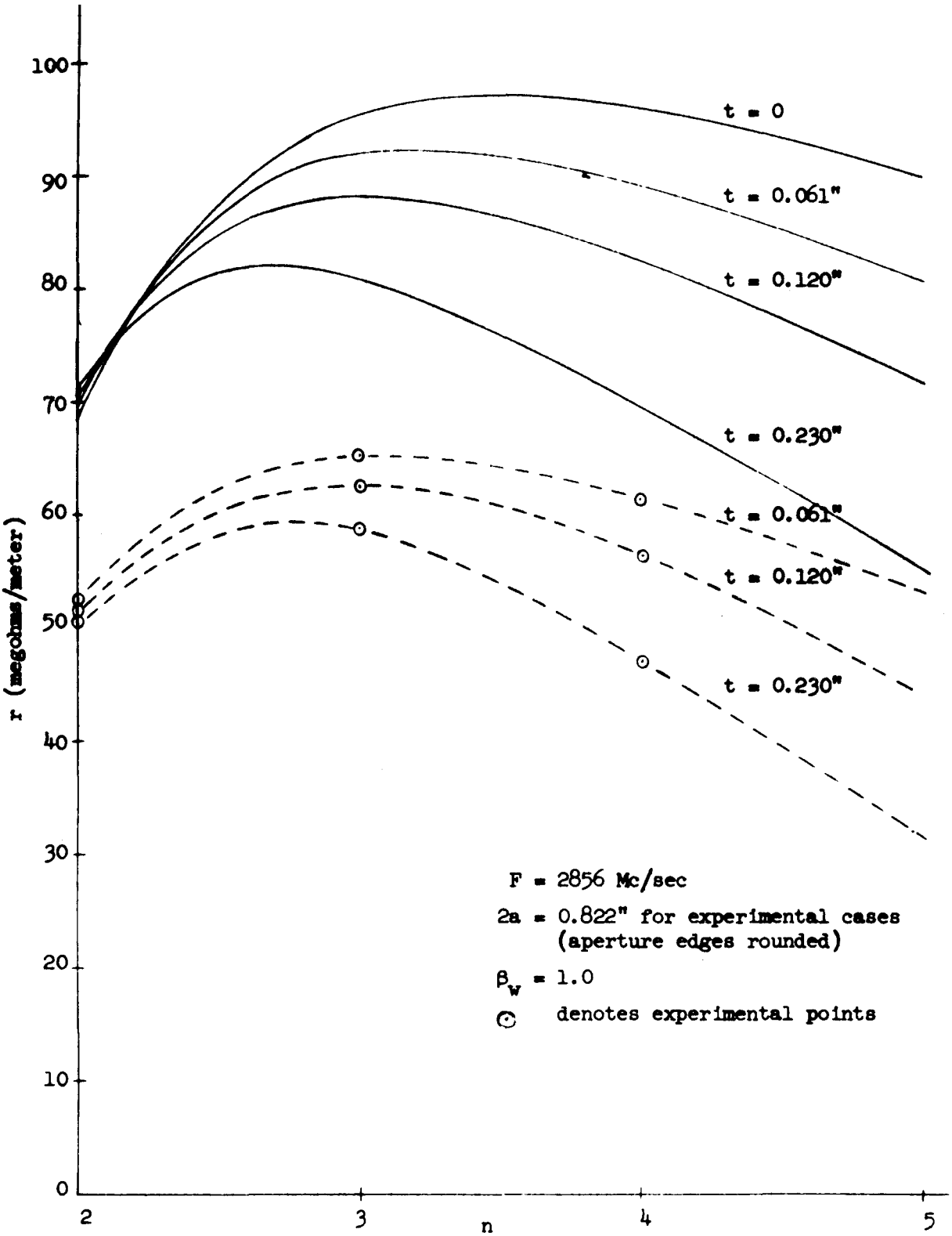

Theoretical and experimental curves of shunt impedance (r) per unit length vs number of disks per wavelength (n) for various disk thicknesses (t).

Fig. 5

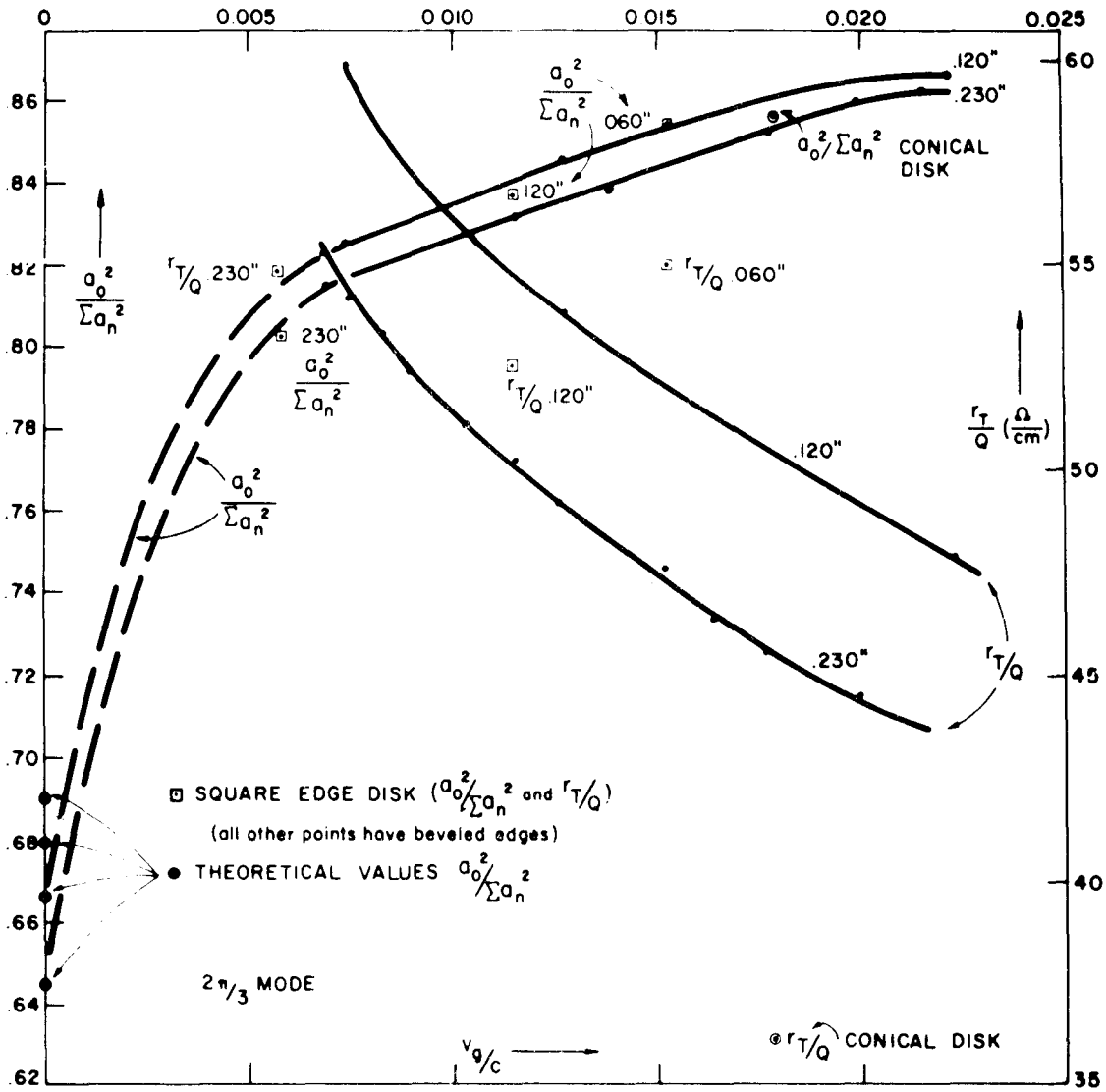

SPACE-HARMONIC AMPLITUDE AND TOTAL r/Q AS A FUNCTION OF NORMALIZED GROUP VELOCITY.
(For various disk thicknesses 0.230, 0.120, and 060)

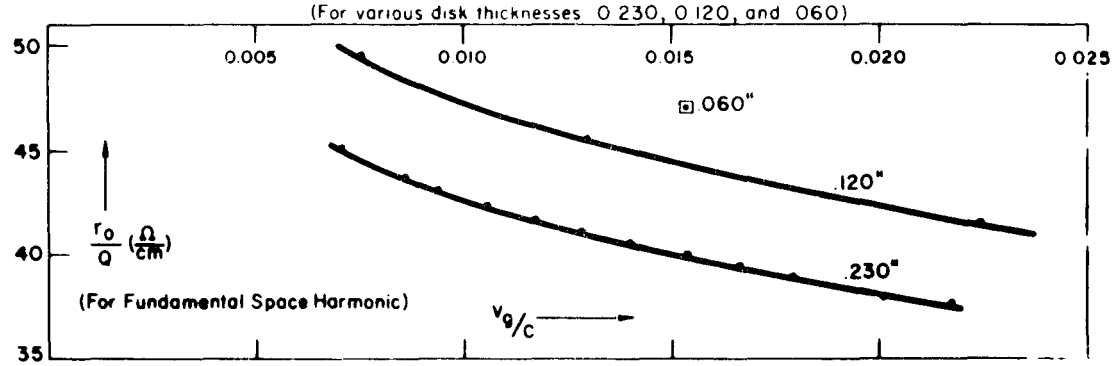

CORRECTED r/Q FOR SPACE HARMONIC AS A FUNCTION OF NORMALIZED GROUP VELOCITY.
(For various disk thicknesses 0.230, 0.120, and .060)

Fig. 6

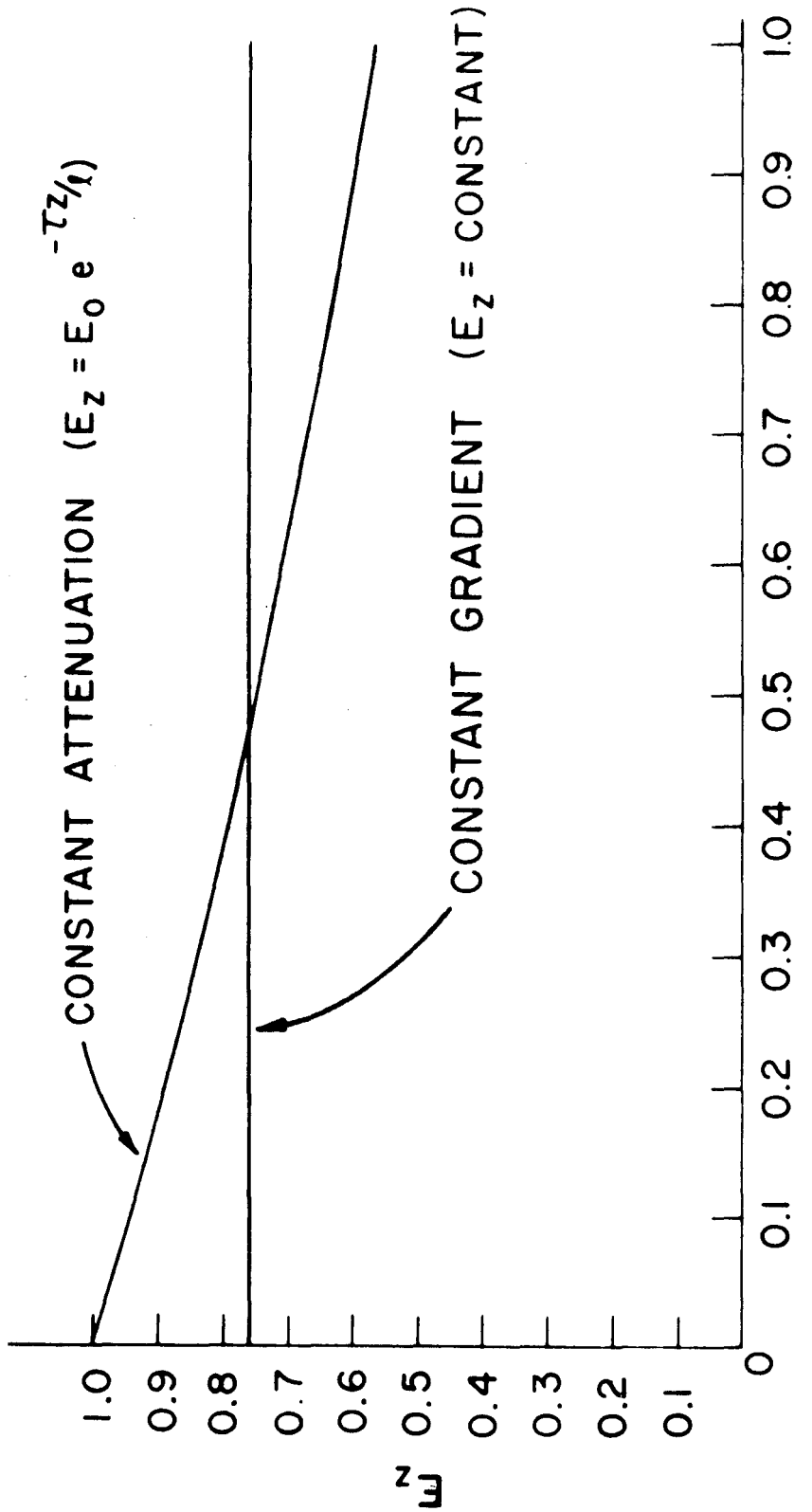

FIG. 4 AXIAL FIELD STRENGTH VERSUS Z FOR EQUAL ELECTRON ENERGY GAIN IN CONSTANT GRADIENT AND CONSTANT ATTENUATION SECTIONS. $\tau = 0.57$

Fig. 7

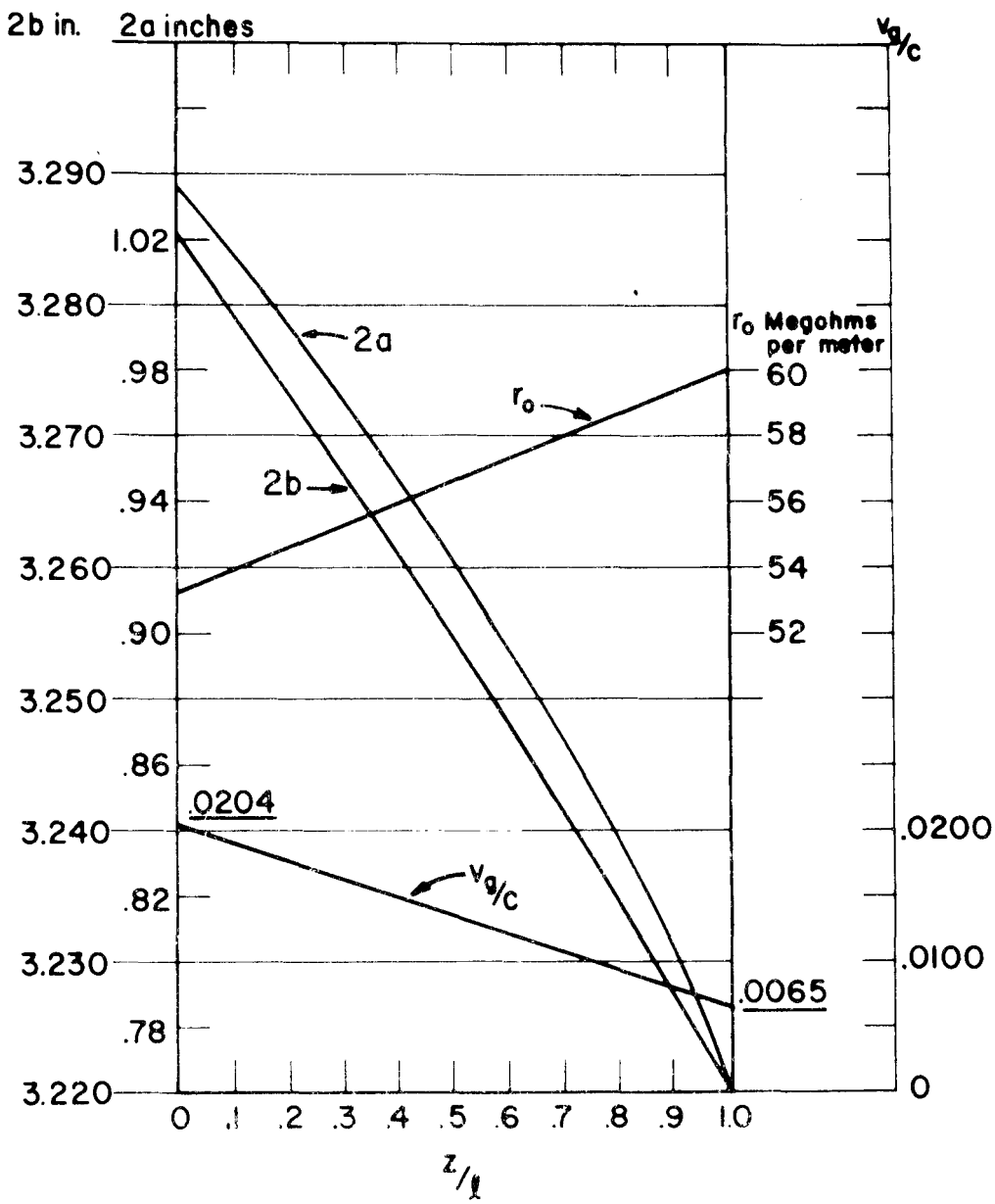

FIG. 8 - VARIATIONS OF 2b, 2a, v_g/c AND THE SHUNT IMPEDANCE r_o (CORRECTED FOR THE FUNDAMENTAL SPACE HARMONIC) AS A FUNCTION OF DISTANCE ALONG A 10-FOOT CONSTANT GRADIENT SECTION FOR $t = 0.230$ INCHES.

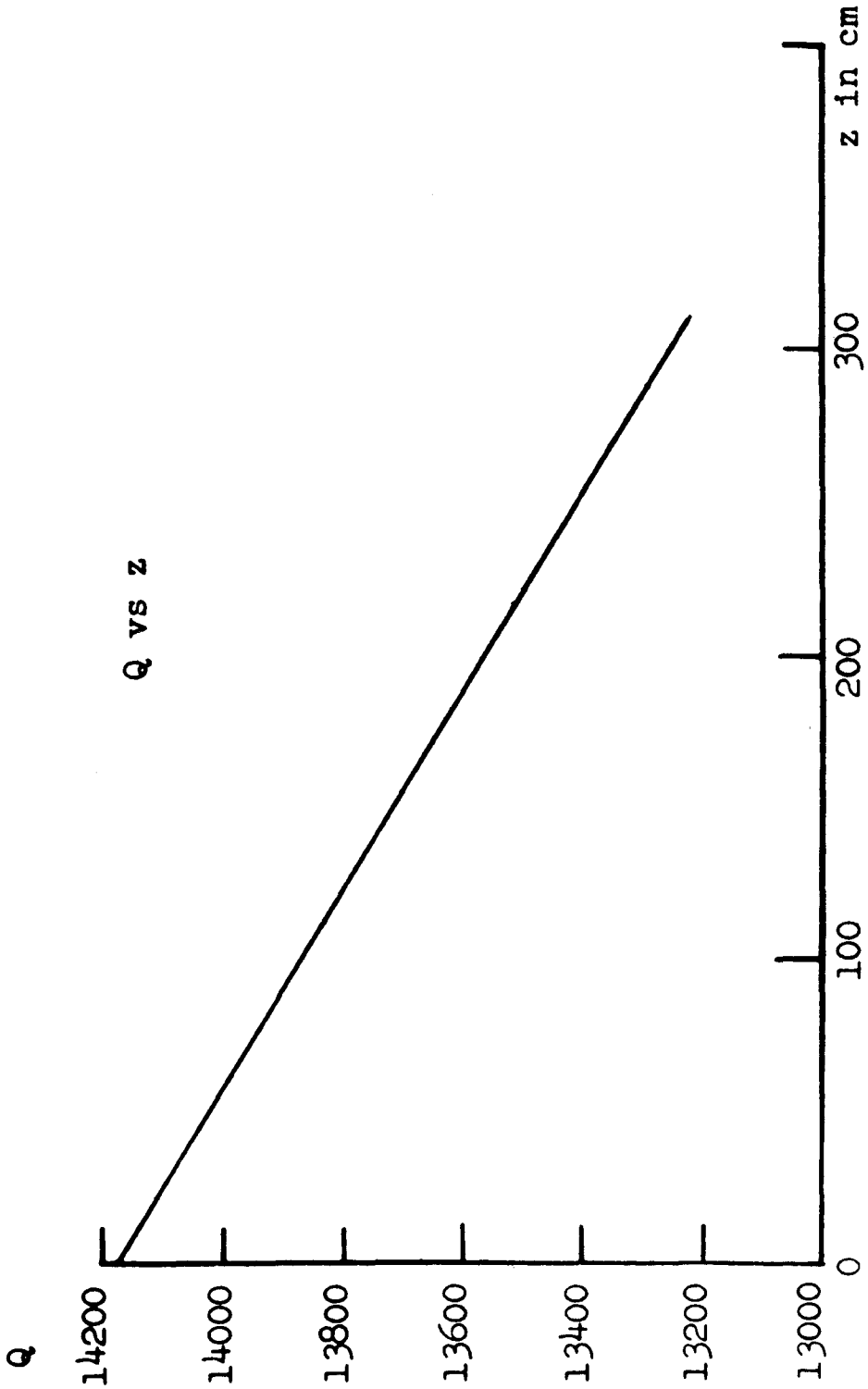

Fig. 9 --Quality factor Q as a function of distance z along constant-gradient section.

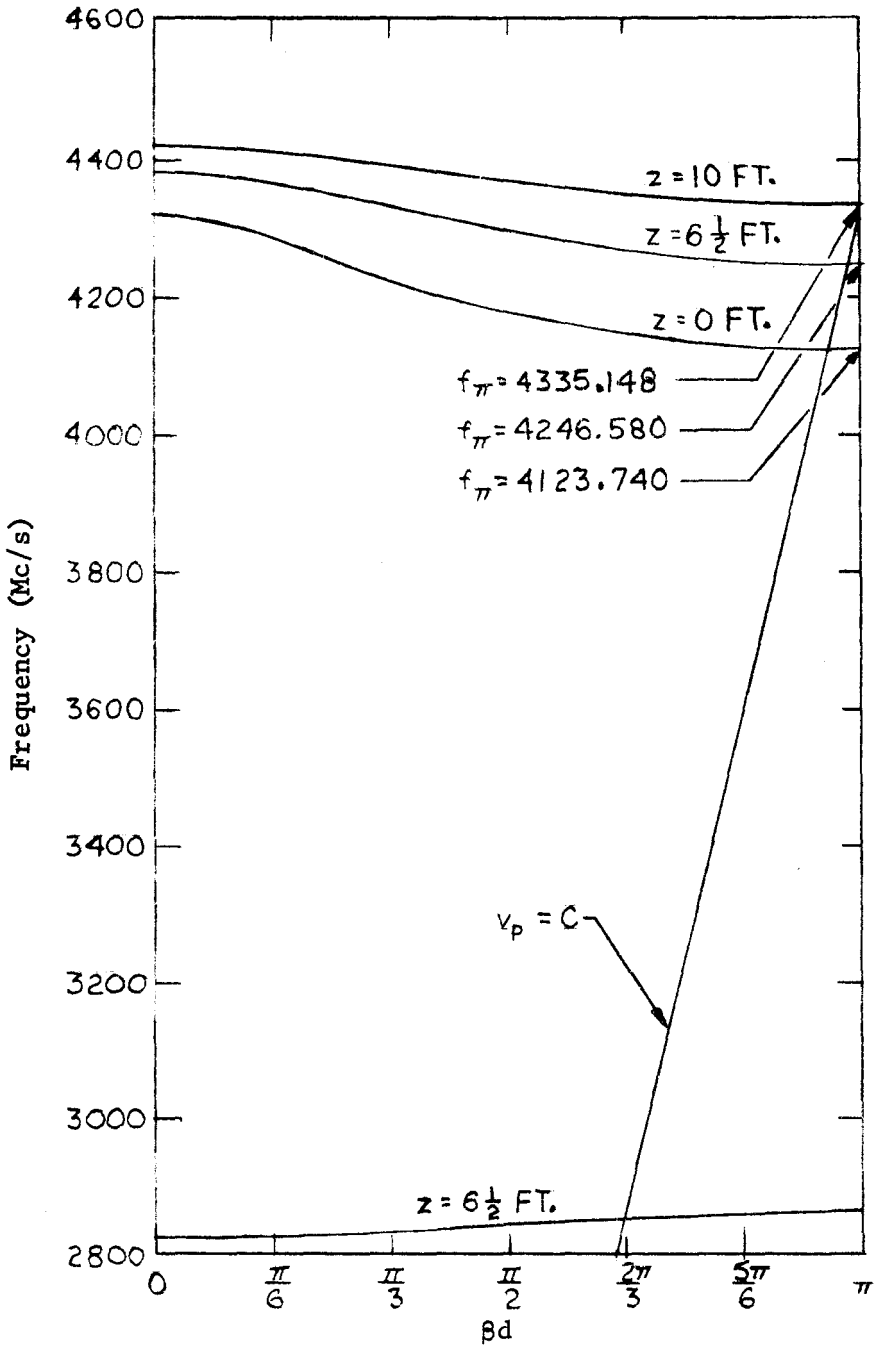

Fig. 10

Effect of the 2π/3 - constant gradient accelerator in avoiding pulse shortening

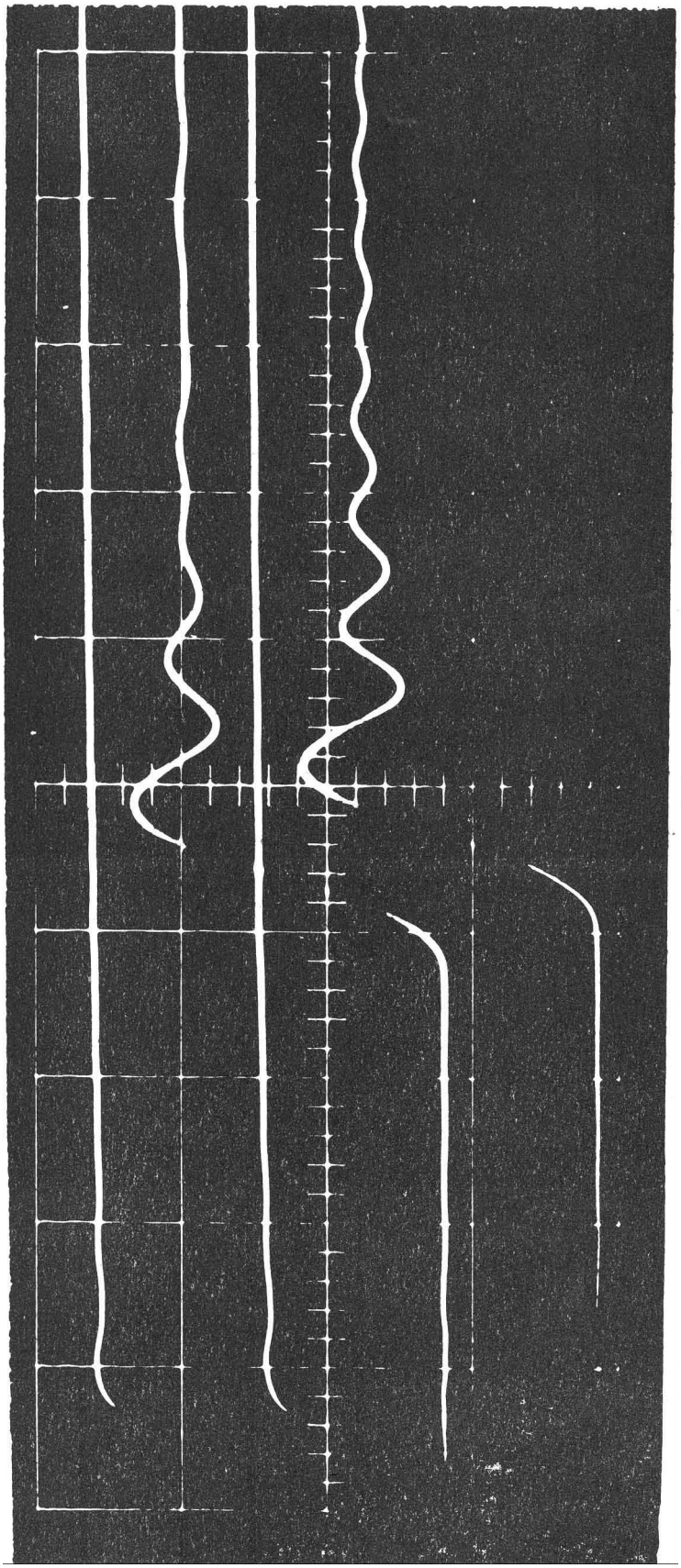

Shapes of input and output rf pulses in a constant gradient accelerator section (upper curves) and a constant impedance accelerator section (lower curves). Length of section = 10 ft, $\tau = 0.57$, and $2\pi/3$ mode in each case. Rise time of input pulse $\cong$ 0.1 μsec; time scale = 0.2 μsec/cm.

Fig. 11

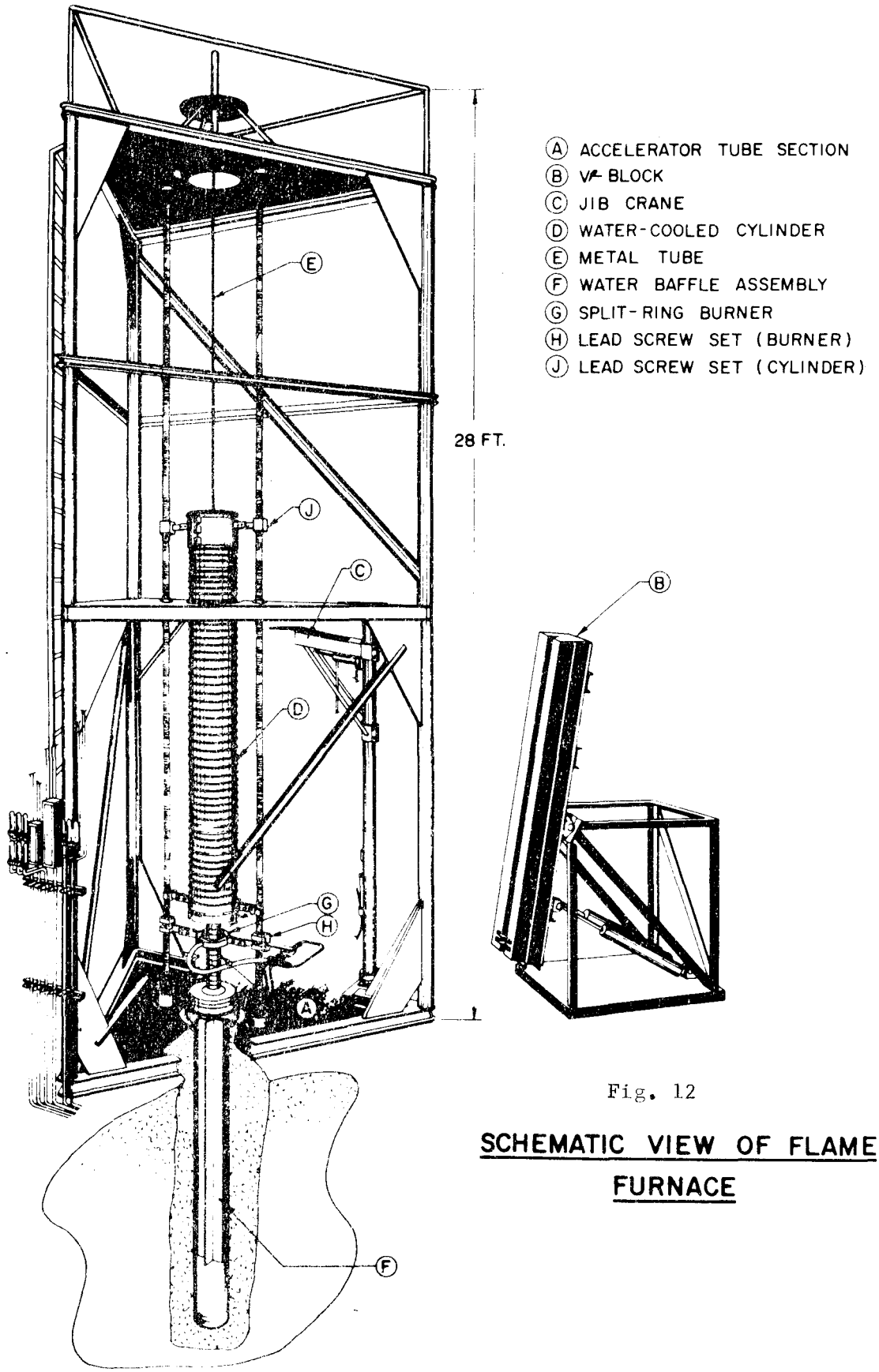

Fig. 12

SCHEMATIC VIEW OF FLAME FURNACE

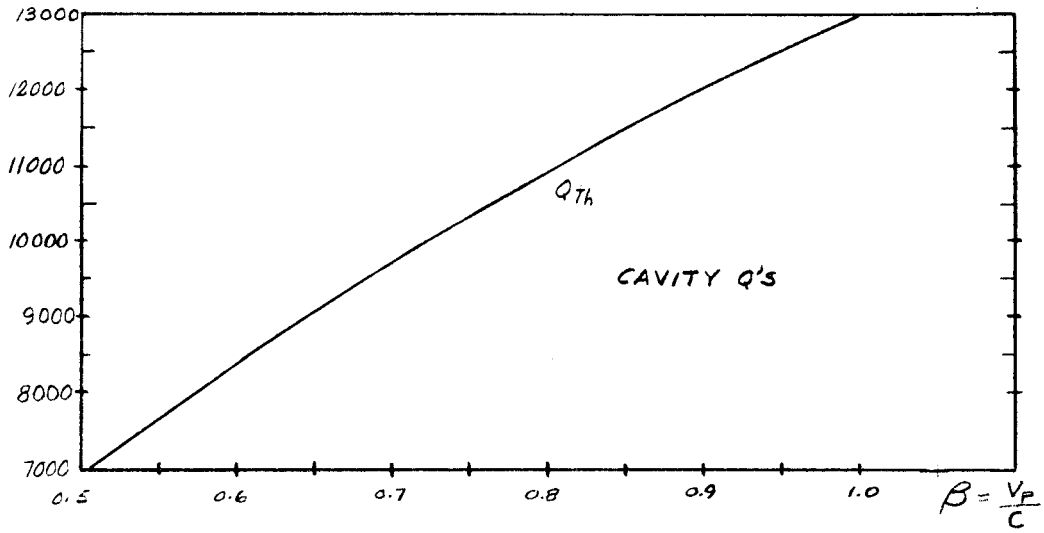
13000
12000
11000
10000
9000
8000
7000
0.5
0.6
0.7
0.8
0.9
1.0
Q_{Th}
CAVITY Q's
$\beta = \frac{V_p}{c}$

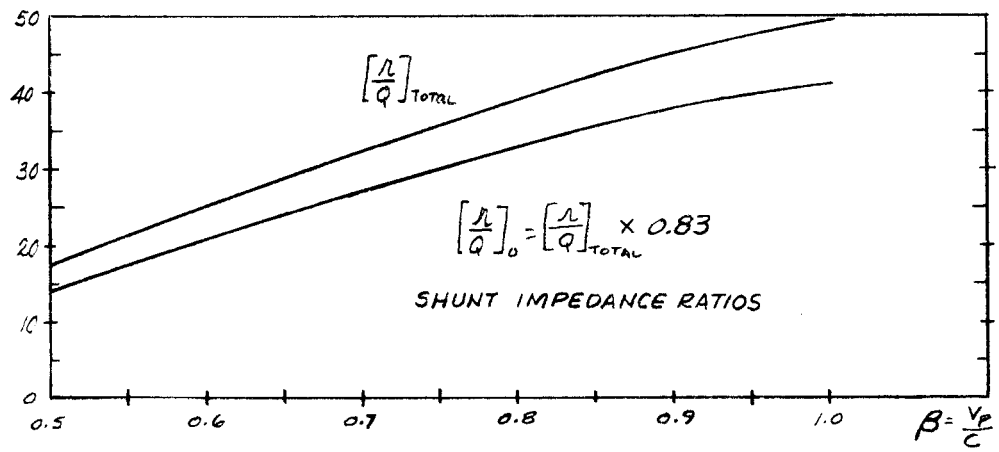
50
40
30
20
10
0
0.5
0.6
0.7
0.8
0.9
1.0
$\left[\frac{r}{Q}\right]_{TOTAL}$
$\left[\frac{r}{Q}\right]_0 = \left[\frac{r}{Q}\right]_{TOTAL} \times 0.83$
SHUNT IMPEDANCE RATIOS
$\beta = \frac{V_p}{c}$

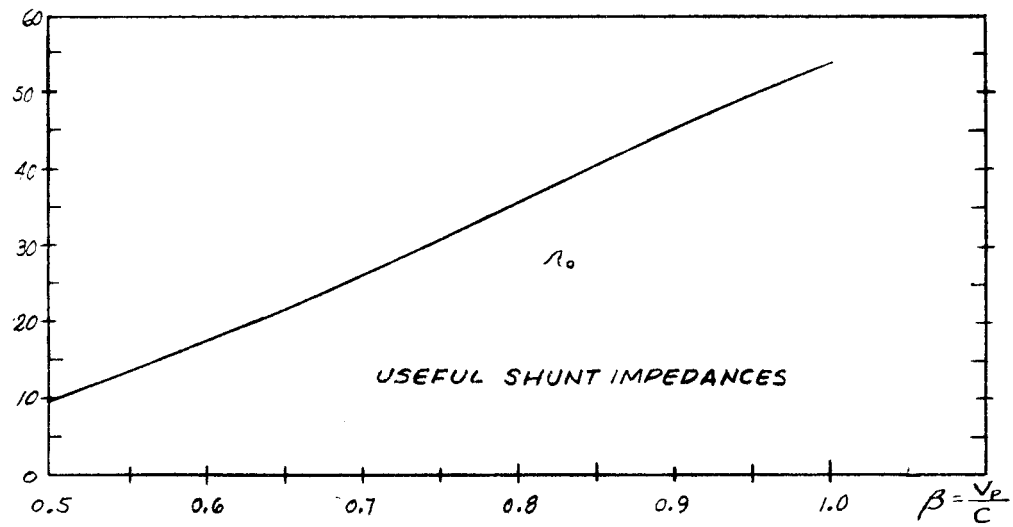
60
50
40
30
20
10
0
0.5
0.6
0.7
0.8
0.9
1.0
r_0
USEFUL SHUNT IMPEDANCES
$\beta = \frac{V_p}{c}$

Fig. 13